Full Paper

Fuel-free nanocap-like motors actuated under visible light

Xu Wang[1]‡, *Varun Sridhar*[1]‡, *Surong Guo*[2], *Nahid Talebi*[2], *Albert Miguel López*[1], *Kersten Hahn*[2], *Peter A. van Aken*[2], *Samuel Sanchez*[1,3,4,]*

[1]Max Planck Institute for Intelligent Systems, Heisenbergstraße 3, 70569 Stuttgart, Germany.

[2]Stuttgart Center for Electron Microscopy, Max Planck Institute for Solid State Research, Heisenbergstraße 1, 70569 Stuttgart, Germany.

[3]Institució Catalana de Recerca i Estudis Avancats (ICREA), Pg. Lluís Companys 23, 08010, Barcelona, Spain.

[4]Institut de Bioenginyeria de Catalunya (IBEC), Baldiri i Reixac 10-12, 08028 Barcelona, Spain.
E-mail: sanchez@is.mpg.de; ssanchez@ibecbarcelona.eu

‡ These authors contributed equally to this work

Keywords: fuel-free nanomotors, visible light, self-electrophoresis, nanomachines, enhanced Brownian motion.

Abstract

The motion of nanomotors triggered by light sources will provide new alternative routes to power nanoarchitectures without the need of chemical fuels. However, most light-driven nanomotors are triggered by UV-light, near infrared reflection (NIR) or laser sources. We demonstrate that nanocap shaped Au/TiO_2 nanomotors (175 nm in diameter) display increased Brownian motion in the presence of broad spectrum visible light. The motion results from the surface plasmon resonance (SPR) effect leading to self-electrophoresis between the Au and TiO_2 layers, a mechanism called plasmonic photocatalytic effect in the field of photocatalysis. This mechanism has been experimentally characterized by electron energy loss spectroscopy (EELS), energy-filtered transmission electron microscopy (EFTEM) and optical video tracking. We also studied this mechanism in a more theoretical manner using numerical finite-difference time-domain (FDTD) simulations. The ability to power nanomaterials with visible light may result in entirely new applications for externally powered micro/nanomotors.

Introduction

Emerging autonomous nano/micromotors are promising man-made devices that could eventually be used in both biomedical and environmental applications.[1] Early research focused on the investigation of catalytic motors, which need chemical components as propellants.[2] The intrinsic biotoxicity of the most widely used fuel, H_2O_2,[3] hinders a much broader application in biomedicine. Although recent reports demonstrated that bio-friendly fuels such as glucose and urea could power nanomotors,[4] the sustained fuel-consumption severely limits the lifetime of such motors. Therefore, external stimuli, including ultrasound,[5] magnetic[6] and electric fields,[7] have been used as fuel-free and biofriendly power sources.

Visible light is becoming an attractive external stimulus to propel nano/micro objects because it represents a ubiquitous and theoretically unlimited fuel source that is non-intrusive, clean, and easily controllable. Most studies to date focused on nano/micromotors powered by non-biocompatible UV light[8] or not easily accessible lasers.[9] To overcome these challenges, a range of nano/micro objects which can use visible light[3b, 10] have been explored. Currently, the reported fuel-free light-driven micromotors rely on two mechanisms: thermophoresis[11] and thermocapillary effects.[12] Surface plasmon resonance (SPR) effects have been developed for photocatalysis applications under visible or UV light,[13] such as photodegradation[14] and photosplitting.[15] In these systems, photocatalytic materials with large band gaps, like TiO_2 (~3.20 eV), are combined with a plasmonic material (gold) to enhance electron transfer in the visible range. Researchers have demonstrated that the catalytic process can be enhanced by charge transfer due to Plasmon induced photocatalytic effects.[16]

We present Au/TiO_2 nanocap motors that display enhanced Brownian motion under visible light through the plasmonic photocatalytic effect. The experimental and simulated localized surface plasmon resonance (LSPR) effect in the Au/TiO_2 nanostructure,[2b, 15b, 16a] coupled with the electric field distribution and thermal diffusion of electrons, induce enhanced Brownian motion of nanocap motors. Materials characterization, theoretical simulations, video tracking analysis of nanomotors and control experiments are presented to confirm the motion of nanocaps in a fuel-free manner. These interpretations are consistent with simulations by Crozier et al.,[17] Yuan et al.[18] and Baffou et al.[19] of metallic nanoparticles containing Au and TiO_2 materials.

Results and Discussion

The Janus nanocaps were fabricated by combining plasma etching and physical vapor deposition methods (Figure 1a). Monolayers of 200 nm polystyrene particles (PS NPs) were prepared by drop casting method and followed by Ar plasma etching to separate the packed PS NPs with nanogaps. Figure panels 1b and c show the obtained monodispersed monolayers of PS NPs.[20] The Au and TiO_2 layers were successively evaporated on the loosely packed PS NPs patterns to form Janus PS/Au/ TiO_2 particles by electron beam deposition. The obtained Janus nanoparticles were annealed at 600 ºC for 1 hour to produce anatase TiO_2 layers. Finally, the removal of PS template by high temperature evaporation results in the nanocap structure (Figure 1d and e). X-Ray diffraction (XRD) measurements show that the annealed nanocaps mainly contain anatase TiO_2 (Figure S1a), which provides a good photo-catalytic performance, while the unannealed nanocaps only contain amorphous TiO_2 (Figure S1b). A scanning electron microscopy (SEM) image of the TiO_2 surface layer of the nanocaps is shown in Figure 1f.

Additionally, we characterized the nanocaps by using electron energy loss spectroscopy (EELS) and transmission electron microscopy (TEM). EELS provides information about the elemental composition of nanocaps and is capable of identifying low atomic number materials such as O in the TiO_2 layers. The outer TiO_2 layer and the inner Au layer formed separately without mixing (Figure 2a). In addition, the elemental mapping clearly shows that no elements other than Ti, O, and Au were present in the structure. This clear separation of TiO_2 and Au was confirmed from TEM images of nanocaps (Figure 2b). High resolution transmission electron microscopy (HRTEM) provides evidence of the crystalline structure of the interface between TiO_2 and Au (Figure 2c) with lattice spacings in the anatase TiO_2 layer of 0.17 nm, 0.23 nm, and 0.163 nm of the (1 0 5), (1 1 2), and (2 1 1) planes, respectively.

In order to demonstrate the Plasmon induced photocatalytic effect, we measure the plasmon resonances of a single Au/TiO_2 nanocap with EELS and energy-filtered transmission electron microscropy (EFTEM). EELS is among the pioneering methods to map plasmons at nanometer scales.[21] EELS is often assumed to to be able to reflect the parameter of photonic local density of states (LDOS)[22] projected along the trajectory of the electron beam. Meanwhile, EFTEM is used to show the spatial distribution of a selected plasmon resonance in a single Au/TiO_2 nanocap. A resonant plasmon peak at 1.75eV (Figure 3a), at both the Au/TiO_2 and TiO_2/vacuum interfaces (Figure 3a), indicates strong absorption around the 708 nm wavelength. Figure 3b presents the spatial distribution of the surface plasmon resonance at 1.2-2.4 eV. The localization areas with higher intensity indicate stronger absorption for that specific energy range.

The calculated electron-energy-loss probability (Figure 3c) could confirm the experimental finding that plasmon resonances at both interfaces have similar energies. However, a slight energy shift of 1.48 eV in the calculated EEL spectra had been expected because the actual dielectric function of the TiO_2 layer and the orientation of the nanocap[23] cannot be exactly determined. The dielectric function of TiO_2 strongly depends on its crystal structure. By means of a numerical FDTD simulation, we could show that this nanocap structure sustained a typical dipolar plasmon mode (Figure 3d). Furthermore, the total electric field of the exited surface plasmons (E_{tot}.) is mostly localized at the outer edge between TiO_2/Vacuum and Au/TiO_2, as well as at the Si_3N_4 substrate below the nanocap/substrate interface. It should be noticed that optical excitation can introduce pressure on the structure. The density of the induced electromagnetic momentum and the stress tensor both depend on the electric field and the magnetic field distributions. Symmetries of the different field components however are not the same; This effect introduces an additional

asymmetry to the induced pressure on the particle. Thus the optical pressure manipulates the motion of the particle dissimilar to the mechanism of heat transfer.

To investigate the influence of this plasmon effect on self-propulsion, a white halogen cold light source (LCD lamp) with an intensity of 100 mW/cm^2 was used to illuminate the samples. Surface plasmon resonance on the Au surface, due to the incident LCD light, excites the free electrons on the metal surface, causing the nanocaps to appear as bright spots on microscope. The higher light intensity means more charges are in oscillation (i.e., excited) on the Au surface, which in turn leads to a more pronounced Plasmon induced photocatalytic effect. Higher light intensities lead to an increased proton gradient and fluid shear velocity, due to the increased fluid flow around the particle caused by higher charge separation (Figure 4a). The light absorption spectrum for the Au/TiO_2 nanocaps showed an absorption peak at 690 nm (Figure 4b).

The plasmonic photocatalytic mechanism results is an increased Brownian motion of the nanocaps upon visible light. The tracking trajectories of representative light-activated nanocaps tracked for 10s are displayed in Figure 4c. In order to observe the nanocaps, we had to use the intensity microscope focus light to illuminate the sample. This means that our "dark" control or baseline (Fig. 4d, e, f) was in fact illuminated with the microscope's 1 mW/cm^2 focus light. The diffusion coefficient (D) is given by $D=MSD/\ i\cdot\Delta t$ and for the case of a two-dimensional Brownian motion analysis, i is equal to 4. The MSD values (in 1 second interval time) for these low (microscope only) and high (microscope plus LCD) light intensities respectively are plotted in Figure 4d. We also tracked 12 Au/TiO_2 nanocaps to investigate how turning LCD light ON and OFF would affect their mobility. The diffusivity of an individual nanocap decreased from 1.87 ± 0.5 μm^2/s (LCD on) to 1.04± 0.2μm^2/s when the LCD light was turned off (Figure 4e). These results

Comentado [SS1]: For how long is the tracking?

provide direct proof of the correlation between increased Brownian motion of nanocap motors and visible light intensity.

Within the plasmonic photocatalytic mechanism, there are two possible contributions that may affect Brownian motion of the nanocaps: (1) electron diffusion between the Au and TiO_2 layers due to electrons in the Au layer becoming excited by the incident visible light, and (2) dissipation of part of the incident light energy as heat and its diffusion into the surrounding fluid.[16a, 16b, 24] In the first mechanism, some separated electrons are lost through recombination and other surface losses, including thermal diffusion of the excited electrons on the Au side, while the remaining electrons are injected into the conduction band of TiO_2. This charge separation creates an electric field around the nanocap. The generated protons from the oxidation of water at the Au layer flow to the surface of TiO_2 and are then reduced by diffused electrons at TiO_2 layer.[8b, 25] The diffusion of proton products due to electron flow between the two layers, can induce a solute flow on the surrounding fluid from the Au inner surface to the TiO_2 outer surface via self-electrophoresis (Figure 4a). This provides a propelling force to move the nanocaps forward. Self-electrophoresis is a process in which the charged microparticles move in a self-generated electric field due to the asymmetric distribution of ions. In previous reports on visible light activated Au/TiO_2 microparticles,[25-26] the electrons produced from the Au layer were transported to and consumed by the exposed TiO_2 surface[26] resulting in a fluid flow towards TiO_2 and thus propulsion of the microparticles. Hong et al.[8b] showed that anatase TiO_2 particles are very active and can move under UV light. The XRD spectrum (Figure S 1a) shows the formation of a uniform anatase phase.

Visible light cause excitation of large amounts of free electrons on the Au layer due to the Plasmon induced photocatalytic effect. This brings about a negative shift in the Fermi energy level of TiO_2. In order to investigate the motion mechanism, we performed three control experiments

(Figure 4f). First, the Au layer was replaced by 20 nm Pt layer to form Pt/TiO_2 nanocaps. Pt nanolayer is not as active as Au when light is incident on it as showed by the weak visible light absorption in Figure S2. Without LCD light, the diffusion coefficient of Pt/TiO_2 nanocaps is 1.31 ± 0.36 $\mu m^2/s$. When light is turned on, their diffusion coefficient slightly increases to 1.45 ± 0.25 $\mu m^2/s$ (Figure 4f). Pt does not show any significant peak in absorption of visible light, thus causing a shallow Plasmon resonance which explains the low diffusion coefficient for Pt/TiO_2 nanocaps and the fact that there is no increase in this diffusion after LCD light ilumination. This experiment indicates that Au as active material, with high absorption visible light band is crucial for the enhanced Brownian motion of the nanocaps via Plasmon photocatalytic effect.

Comentado [SS2]: Pt absorption was too low and produces a shallow plasmon

In another control experiment, we synthesized nanocaps composed of 20 nm Au, 10 nm SiO_2, and 25 nm TiO_2 layers. Here, the SiO_2 sandwiched layer separates the direct contact between Au and TiO_2 blocking the flow of electrons, which leads to a blue shift compared to the UV-vis absorption peak of 20 nm Au/25 nm TiO_2 nanocaps (Figure S2). When LCD light is on, the diffusion coefficient value is increased slightly from 0.84 ± 0.26 $\mu m^2/s$ to 0.9 ± 0.24 $\mu m^2/s$ (Figure 4f) with no significant differences, which is much lower than the values obtained with the TiO_2/Au nanomotors. These two controls prove the effect of Plasmon induced electron flow in the TiO_2/Au nanomotors.

The second contributor to the motion relies on the rapid heat transfer away from the water-Au interface aiding the nanocap movement through thermophoresis. An average temperature increase of 0.2 ± 0.05°C was detected in the bulk solution (Figure S4) when LCD light was turned on the nanocaps. We fabricated Au/ SiO_2 nanocaps as the control samples to evaluate the thermophoretic effect of light-driven nanomotors ruling out the Plasmonic photocatalytic effect effect as the SiO_2 layer can prevent hot electrons transport from Au layer. The light absorption spectra of these

modified nanocaps clearly show that Au/SiO_2 and Au/amorphous TiO_2 nanocaps do not have the ability to absorb visible light (red and blue curves in Figure S2). We measured the diffusion coefficient value of the Au/SiO_2 nanomotors (Figure 4f) by tracking them under LCD light is 0.98 ± 0.08 $\mu m^2/s$, which is almost the same as the value without LCD light (0.97 ± 0.07 $\mu m^2/s$) with no significant differences. These results indicate that, at this light power and wavelength, the thin Au layer on the nanocaps is not sufficient to provoke an enhanced Brownian motion and hence the thermophoresis is in this case not a significant effect.

Conclusions

We demonstrated that Au/TiO_2 nanocaps exhibit active Brownian motion when illuminated by an LCD light, thus becoming nanomotors that were activated by visible light. The mechanism for the motors' propulsion was interpreted as the fast electron transfer between the two layers of the nanocaps leading to a self-electrophoresis effect under visible light. Both, the experimental and the simulation results of Au/TiO_2 plasmon resonance absorption supported this proposed motion mechanism. It was found that these photoactive nanocaps react to changes in light intensity produced by an LCD lamp when light was turned on and off. This work provides a novel structure and fabrication technique which could be used for the activation and manipulation of biocompatible nano/micro machines, merely requiring visible light as a propulsion mechanism.

Experimental Section

Fabrication of Nanocaps. 175 nm Au/TiO_2 nanocaps were fabricated by electron beam physical vapor (E-beam) deposition and annealing. A polystyrene monodispersed particle (Sigma-Aldrich)

monolayer was prepared by drop casting method with 200 nm PS in ethanol solution. Followed by an argon plasma etching process (60 W radio frequency power with 0.5 mm Hg),[20] PS particles were separated from one another and their sizes were reduced to 130 nm. Then, 20 nm Au and 30 nm TiO_2 layers from pure Au and TiO_2 pellets (Kurt J. Lesker Company) were deposited on the upper surface of the PS monolayer. After annealing for 1h at 600 °C, amorphous TiO_2 was turned to Anatase TiO_2 and PS templates were removed. Finally, Au/TiO_2 nanocaps on silicon wafer were collected with DI water by 30 min ultrasound sonication. 175 nm Pt/TiO_2 nanocaps were prepared with the same method by using Pt pellets instead of Au. For 185 nm Au/SiO_2/TiO_2 nanocaps, 20 nm Au, 10 nm SiO_2 and 35 nm TiO_2 layers were deposited on 100 nm PS monolayer sequentially before 1 h annealing process in 600°C oven. 175 nm Au/SiO_2 and Au/amorphous TiO_2 nanocaps were prepared by E-beam deposition with 20 nm Au/25 nm SiO_2 and 20 nm Au/25 nm TiO_2 layers which were then washed with DMF solution to remove PS templates.

Instruments

Images of PS particles, Janus structures, and nanocaps were captured by a Zeiss ULTRA 55 SEM. HRTEM and STEM-EELS spectra were recorded in a Jeol ARM 200F-DCOR equipped with a field-emission electron source, a probe Cs corrector, and a Gatan GIF Quantum ERS spectrometer. EFTEM imaging, and EELS measurements were conducted with the Zeiss SESAM microscope. The microscope was equipped with an electron monochromator (CEOS Heidelberg) and the MANDOLINE energy filter. Optical videos were recorded by Leica optical microscopy. The KL 1500 LCD (SCHOTT) close to 100 CRI halogen spectrum and original focus light from Leica optical microscopy were used as illuminators. Testo 85-infrared Thermometer was used to detect the temperature changes of Au/TiO_2 nanocaps. DLS measurements were operated by Malvern Zetasizer Nano ZS.

SPR Peak Absorption and FDTD Simulation

EELS data were acquired with an energy resolution of 90 meV as determined from the full width at half maximum of the zero-loss peak (ZLP). The acquisition time for each spectrum was 0.8 s. The energy-loss spectrum was dispersed perpendicular to the energy-dispersive direction on the CCD camera in order to make the full dynamic range of almost 1000 between ZLP and plasmon peaks accessible without saturating the camera.

In order to perform the simulations, a numerical finite-difference time-domain (FDTD) method was used.[27] The whole simulation domain was discretized with unit cells of 1.5 nm edge, and a higher-order absorbing boundary condition has been exploited to meet the far-field radiation boundary conditions. In order to model the permittivity of both gold and TiO_2, a Drude model in addition to two critical-point functions has been introduced into the simulation domain.[28]

Author Contributions

X.W., V.S. and S.S. initiated the project. X.W. and V.S. prepared the nanocaps and carried out the experiments. S. G., N.T. and P.v.A. provided the plasmon-related experiment and simulation results. K.H. conducted the TEM imaging and EELS mapping. A. M.L. developed a code for tracking nanocaps and analyzed their motion. All the authors contributed to the paper writing. Author 1 and Author 2 contributed equally to this work.

Acknowledgements

The research leading to these results has received funding from the European Research Council under the European Union's Seventh Framework Program (FP7/20072013)/ERC grant agreement no. 311529 (LT-NRBS). The authors thank Prof. Fischer for E-beam deposition instrument support. We also thank Prof. E. J. Mittemeijer for the XRD measurements.

Figures

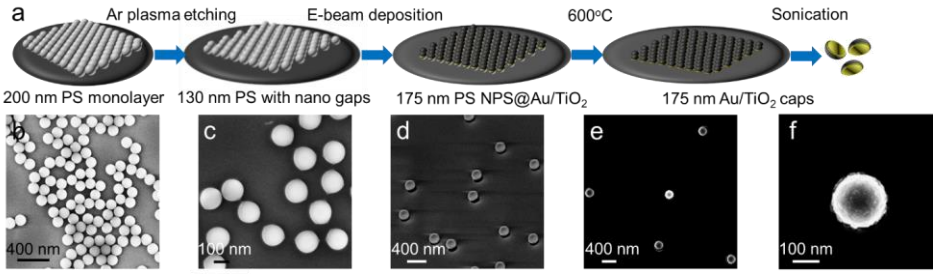

Figure 1. Fabrication of nanocaps. (a) Schematic of the multi-step fabrication procedure of 175 nm Au/TiO_2 nanocaps. (b-f) Scanning electron microscope images of (b) 200 nm polystyrene particles (PS), (c) loosely packed PS film after Ar plasma etching, (d) Janus $PS/Au/TiO_2$ particles after E-beam deposition, (e) Au/TiO_2 nanocaps without PS after annealing process, and (f) a single Au/TiO_2 nanocap.

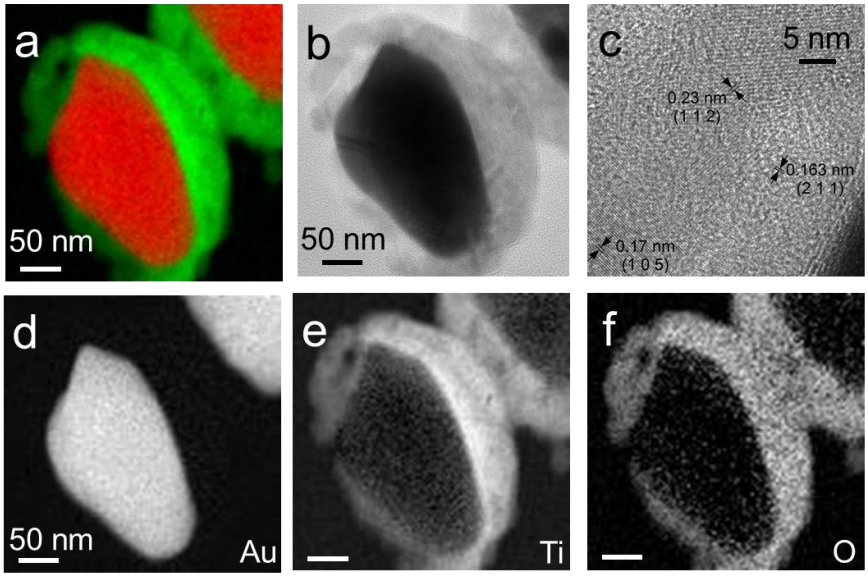

Figure 2. Characterization of nanocaps motors. (a) color-coded elemental map of Au (red, cf. panel d) and Ti (green, cf. panel e). (b) HRTEM image of the 175 nm nanocap with the 20 nm Au core layer shown as dark grey Au surrounded by the 25 nm TiO_2 shell layer (light grey). (c) HRTEM image of the interface between Au and the TiO_2 layer at high magnification. (d–f) EELS spectrum images of (d) Au-$M_{4,5}$ at 2206 eV, (e) Ti-$L_{2,3}$ at 455 eV, and (f) O-K at 532 eV.

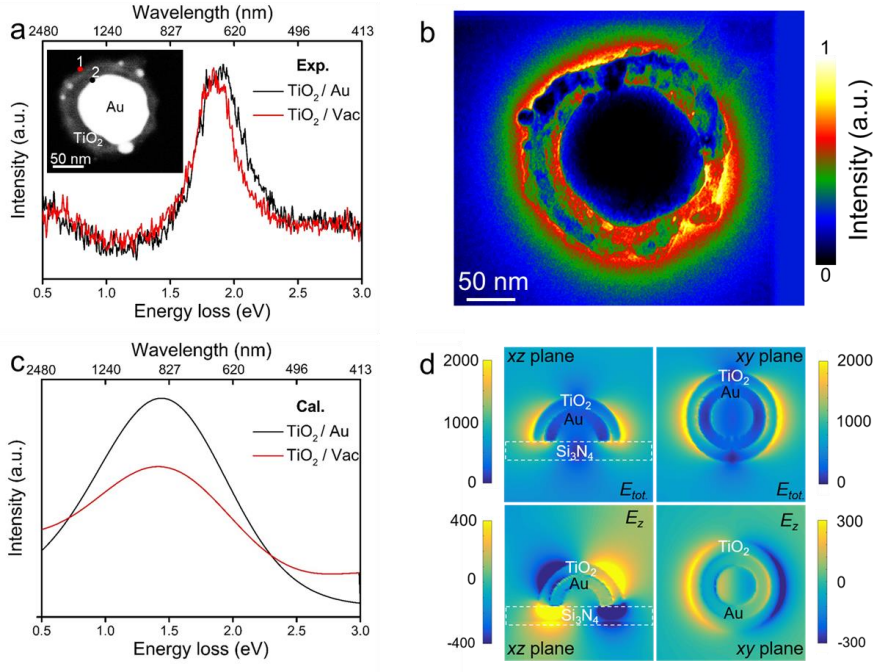

Figure 3. (a) Experimental EEL spectra (zero-loss peak corrected) at the interfaces of Au/TiO_2 and TiO_2/Vacuum. The inset shows the STEM-HAADF image of a single Au/TiO_2 nanocap and the two highlighted spots indicate the considered impact parameters. (b) 1.2-2.4 eV energy-filtered TEM image of a single Au/TiO_2 nanocap. (c) Calculated electron-energy-loss probability at the interfaces of Au/TiO_2 and TiO_2/Vacuum. (d) Spatial distribution of the calculated total

electric field (color code) $E_{tot.} = \sqrt{|E_x|^2 + |E_y|^2 + |E_z|^2}$ and E_z in the *xz* and *xy* planes (above the substrate) of a single Au/TiO_2 nanocap when the structure is excited with linearly polarized light along the *x*-direction at 1.5 eV. The structure is above a 30 nm-thick Si_3N_4 substrate in FDTD simulations, as in our EELS and EFTEM measurements.

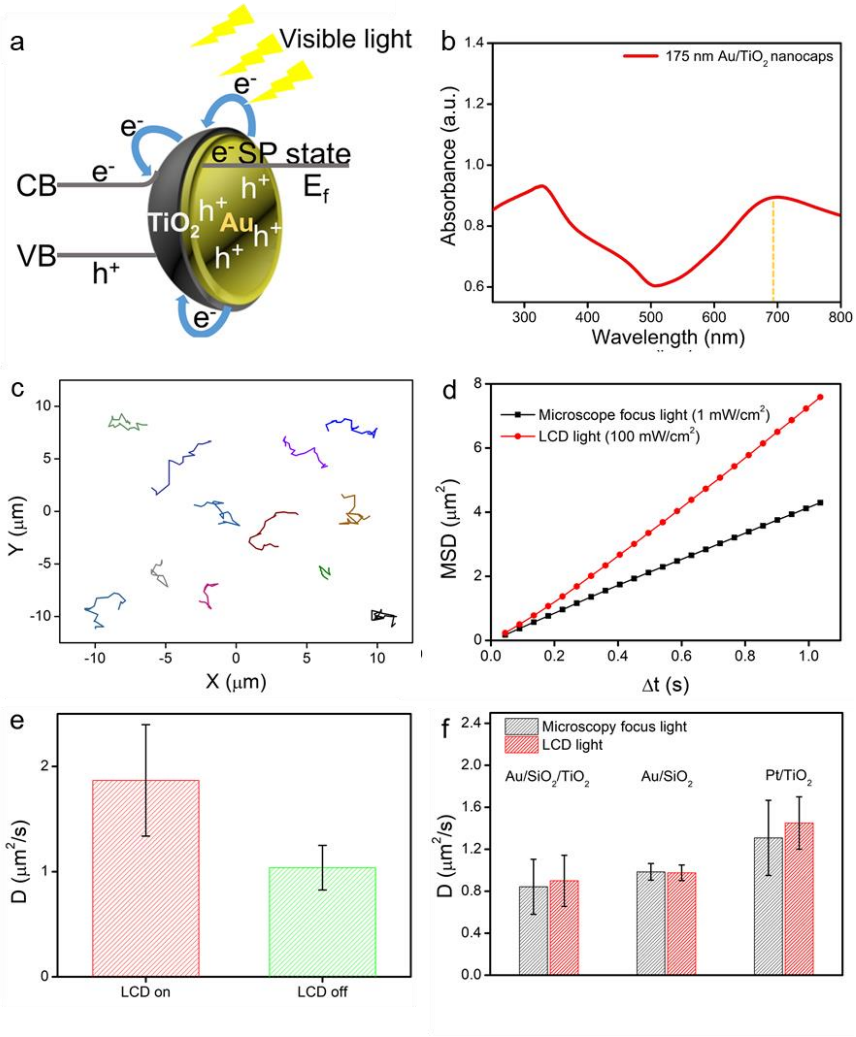

Figure 4. Enhanced Brownian motion of nanocaps. (a) Schematic cartoon for the surface plasmon resonance effect of Au/TiO_2 under visible light. (b) Light absorption spectrum of 175 nm Au/TiO_2 nanocaps. (c) Trajectory of 12 nanocaps with X and Y coordinates under LCD light tracked for 10s. (d) Average MSD versus time interval (Δt=1 s) for 12 tracked 175 nm nanocaps with and without LCD light (100 mW/cm^2). (e) Diffusion coefficient for 12 Au/TiO_2 nanomotors with cycled LCD light (on/off). Each track corresponds to 8 s. (f) Average diffusion coefficient values of $Au/SiO_2/TiO_2$, Au/SiO_2, Pt/TiO_2 nanocaps with focus light (1 mW/cm^2) and LCD light (100 mW/cm^2).

References

[1] a) J. Wang, *ACS Nano* **2009**, 3, 4; b) S. Sengupta, M. E. Ibele, A. Sen, *Angewandte Chemie International Edition* **2012**, 51, 8434; c) M. Guix, C. C. Mayorga-Martinez, A. Merkoçi, *Chemical Reviews* **2014**, 114, 6285; d) S. Sánchez, L. Soler, J. Katuri, *Angewandte Chemie International Edition* **2015**, 54, 1414; e) H. Wang, M. Pumera, *Chemical Reviews* **2015**, 115, 8704; f) J. Katuri, X. Ma, M. M. Stanton, S. Sánchez, *Accounts of chemical research* **2016**, 50, 2; g) F. Wong, K. K. Dey, A. Sen, *Annual Review of Materials Research* **2016**, 46, 407; h) P. Illien, R. Golestanian, A. Sen, *Chemical Society Reviews* **2017**.

[2] a) R. F. Ismagilov, A. Schwartz, N. Bowden, G. M. Whitesides, *Angewandte Chemie International Edition* **2002**, 41, 652; b) V. Subramanian, E. E. Wolf, P. V. Kamat, *Journal of the American Chemical Society* **2004**, 126, 4943; c) H. Wang, G. Zhao, M. Pumera, *Journal of the American Chemical Society* **2014**, 136, 2719.

[3] a) Y. Li, F. Mou, C. Chen, M. You, Y. Yin, L. Xu, J. Guan, *RSC Advances* **2016**, 6, 10697; b) D. Zhou, Y. C. Li, P. Xu, N. S. McCool, L. Li, W. Wang, T. E. Mallouk, *Nanoscale* **2017**, 9, 75.

[4] a) D. Pantarotto, W. R. Browne, B. L. Feringa, *Chemical Communications* **2008**, DOI: 10.1039/B715310D1533; b) X. Ma, A. C. Hortelao, A. Miguel-López, S. Sánchez, *Journal of the American Chemical Society* **2016**, DOI: 10.1021/jacs.6b06857; c) X. Ma, X. Wang, K. Hahn, S. Sánchez, *ACS Nano* **2016**, 10, 3597.

[5] a) W. Wang, L. A. Castro, M. Hoyos, T. E. Mallouk, *ACS Nano* **2012**, 6, 6122; b) V. Garcia-Gradilla, S. Sattayasamitsathit, F. Soto, F. Kuralay, C. Yardimci, D. Wiitala, M. Galarnyk, J. Wang, *Small* **2014**, 10, 4154.

[6] a) P. Fischer, A. Ghosh, *Nanoscale* **2011**, 3, 557; b) L. Baraban, R. Streubel, D. Makarov, L. Han, D. Karnaushenko, O. G. Schmidt, G. Cuniberti, *ACS nano* **2013**, 7, 1360; c) F. Qiu, S. Fujita, R. Mhanna, L. Zhang, B. R. Simona, B. J. Nelson, *Advanced Functional Materials* **2015**, 25, 1666; d) B. Jang, E. Gutman, N. Stucki, B. F. Seitz, P. D. Wendel-García, T. Newton, J. Pokki, O. Ergeneman, S. Pané, Y. Or, *Nano letters* **2015**, 15, 4829; e) S. Kim, S. Lee, J. Lee, B. J. Nelson, L. Zhang, H. Choi, *Scientific reports* **2016**, 6, 30713; f) X. Yan, Q. Zhou, M. Vincent, Y. Deng, J. Yu, J. Xu, T. Xu, T. Tang, L. Bian, Y.-X. J. Wang, K. Kostarelos, L. Zhang, *Science Robotics* **2017**, 2; g) X. Z. Chen, M. Hoop, N. Shamsudhin, T. Huang, B. Ozkale, Q. Li, E. Siringil, F. Mushtaq, L. Di Tizio, B. J. Nelson, S. Pane, *Adv Mater* **2017**, 29; h) T. Li, J. Li, K. I. Morozov, Z. Wu, T. Xu, I. Rozen, A. M. Leshansky, L. Li, J. Wang, *Nano Letters* **2017**, 17, 5092.

[7] G. Loget, A. Kuhn, *Nat Commun* **2011**, 2, 535.

[8] a) M. Ibele, T. E. Mallouk, A. Sen, *Angewandte Chemie International Edition* **2009**, 48, 3308; b) Y. Hong, M. Diaz, U. M. Córdova-Figueroa, A. Sen, *Advanced Functional Materials* **2010**, 20, 1568; c) B. Dai, J. Wang, Z. Xiong, X. Zhan, W. Dai, C.-C. Li, S.-P. Feng, J. Tang, *Nature nanotechnology* **2016**, 11, 1087; d) M. Enachi, M. Guix, V. Postolache, V. Ciobanu, V. M. Fomin, O. G. Schmidt, I. Tiginyanu, *Small* **2016**, 12, 5497; e) W. Li, X. Wu, H. Qin, Z. Zhao, H. Liu, *Advanced Functional Materials* **2016**, 26, 3164; f) C. R. Chen, F. Z. Mou, L. L. Xu, S. F. Wang, J. G. Guan, Z. P. Feng, Q. W. Wang, L. Kong, W. Li, J. Wang, Q. J. Zhang, *Advanced Materials* **2017**, 29; g) J. Simmchen, A. Baeza, A. Miguel‐Lopez, M. M. Stanton, M. Vallet‐Regi, D. Ruiz‐Molina, S. Sánchez, *ChemNanoMat* **2017**, 3, 65.

[9] a) B. Qian, D. Montiel, A. Bregulla, F. Cichos, H. Yang, *Chemical Science* **2013**, 4, 1420; b) A. P. Bregulla, H. Yang, F. Cichos, *ACS Nano* **2014**, 8, 6542; c) Z. Wu, X. Lin, Y. Wu, T. Si, J. Sun, Q. He, *ACS Nano* **2014**, 8, 6097; d) J. Shao, M. Xuan, L. Dai, T. Si, J. Li, Q. He, *Angewandte Chemie International Edition* **2015**, 54, 12782; e) M. Xuan, Z. Wu, J. Shao, L. Dai, T. Si, Q. He, *J Am Chem Soc* **2016**, 138, 6492.

[10] a) M. J. Esplandiu, A. Afshar Farniya, A. Bachtold, *ACS nano* **2015**, 9, 11234; b) R. Dong, Y. Hu, Y. Wu, W. Gao, B. Ren, Q. Wang, Y. Cai, *Journal of the American Chemical Society* **2017**, 139, 1722; c) B. Jang, A. Hong, H. E. Kang, C. Alcantara, S. Charreyron, F. Mushtaq, E. Pellicer, R. Büchel, J. Sort, S. S. Lee, B. J. Nelson, S. Pané, *ACS Nano* **2017**, 11, 6146; d) J. Wang, Z. Xiong, X. Zhan, B. Dai, J. Zheng, J. Liu, J. Tang, *Adv Mater* **2017**, 29.

[11] a) H.-R. Jiang, N. Yoshinaga, M. Sano, *Physical Review Letters* **2010**, 105, 268302; b) M. Yang, M. Ripoll, *Soft Matter* **2014**, 10, 1006.

[12] C. Maggi, F. Saglimbeni, M. Dipalo, F. De Angelis, R. Di Leonardo, *Nat Commun* **2015**, 6.

[13] a) S. Linic, P. Christopher, D. B. Ingram, *Nat Mater* **2011**, 10, 911; b) W. Hou, S. B. Cronin, *Advanced Functional Materials* **2013**, 23, 1612.

[14] K. Awazu, M. Fujimaki, C. Rockstuhl, J. Tominaga, H. Murakami, Y. Ohki, N. Yoshida, T. Watanabe, *Journal of the American Chemical Society* **2008**, 130, 1676.

[15] a) Z. Liu, W. Hou, P. Pavaskar, M. Aykol, S. B. Cronin, *Nano Letters* **2011**, 11, 1111; b) Z. W. Seh, S. Liu, M. Low, S.-Y. Zhang, Z. Liu, A. Mlayah, M.-Y. Han, *Advanced Materials* **2012**, 24, 2310; c) S. C. Warren, E. Thimsen, *Energy & Environmental Science* **2012**, 5, 5133; d) X.-C. Ma, Y. Dai, L. Yu, B.-B. Huang, *Light: Science & Applications* **2016**, 5, e16017.
[16] a) Y. Tian, T. Tatsuma, *Journal of the American Chemical Society* **2005**, 127, 7632; b) A. Furube, L. Du, K. Hara, R. Katoh, M. Tachiya, *Journal of the American Chemical Society* **2007**, 129, 14852; c) S. Linic, U. Aslam, C. Boerigter, M. Morabito, *Nat Mater* **2015**, 14, 567.
[17] a) K. Wang, E. Schonbrun, K. B. Crozier, *Nano Letters* **2009**, 9, 2623; b) K. Wang, E. Schonbrun, P. Steinvurzel, K. B. Crozier, *Nat Commun* **2011**, 2, 469.
[18] C. Min, Z. Shen, J. Shen, Y. Zhang, H. Fang, G. Yuan, L. Du, S. Zhu, T. Lei, X. Yuan, *Nat Commun* **2013**, 4.
[19] G. Baffou, C. Girard, R. Quidant, *Physical Review Letters* **2010**, 104, 136805.
[20] L. Yan, K. Wang, J. Wu, L. Ye, *The Journal of Physical Chemistry B* **2006**, 110, 11241.
[21] M. Kociak, O. Stephan, *Chemical Society Reviews* **2014**, 43, 3865.
[22] F. J. García de Abajo, M. Kociak, *Physical Review Letters* **2008**, 100, 106804.
[23] R. Jiang, F. Qin, Y. Liu, X. Y. Ling, J. Guo, M. Tang, S. Cheng, J. Wang, *Advanced Materials* **2016**, 28, 6322.
[24] L. Du, A. Furube, K. Hara, R. Katoh, M. Tachiya, *Journal of Photochemistry and Photobiology C: Photochemistry Reviews* **2013**, 15, 21.
[25] C. Clavero, *Nat Photon* **2014**, 8, 95.
[26] M. Serra, J. Albero, H. García, *ChemPhysChem* **2015**, 16, 1842.
[27] a) T. Nahid, S. Wilfried, V. Ralf, A. Peter van, *New Journal of Physics* **2013**, 15, 053013; b) T. Nahid, *New Journal of Physics* **2014**, 16, 053021.
[28] N. Talebi, M. Shahabadi, W. Khunsin, R. Vogelgesang, *Opt. Express* **2012**, 20, 1392.